First principles calculation of electron-phonon and alloy scattering in strained SiGe

F. Murphy-Armando and S. Fahy

Citation: J. Appl. Phys. **110**, 123706 (2011); doi: 10.1063/1.3669446
View online: http://dx.doi.org/10.1063/1.3669446
View Table of Contents: http://jap.aip.org/resource/1/JAPIAU/v110/i12
Published by the American Institute of Physics.

First principles calculation of electron-phonon and alloy scattering in strained SiGe

F. Murphy-Armando[1,a)] and S. Fahy[1,2]
[1]*Tyndall National Institute, University College Cork, Lee Maltings, Cork, Ireland*
[2]*Department of Physics, University College, Cork, Ireland*

(Received 6 September 2011; accepted 11 November 2011; published online 20 December 2011)

First-principles electronic structure methods are used to predict the mobility of *n*-type carrier scattering in strained SiGe. We consider the effects of strain on the electron-phonon deformation potentials and the alloy scattering parameters. We calculate the electron-phonon matrix elements and fit them up to second order in strain. We find, as expected, that the main effect of strain on mobility comes from the breaking of the degeneracy of the six Δ and L valleys, and the choice of transport direction. The non-linear effects on the electron-phonon coupling of the Δ valley due to shear strain are found to reduce the mobility of Si-like SiGe by 50% per % strain. We find increases in mobility between 2 and 11 times that of unstrained SiGe for certain fixed Ge compositions, which should enhance the thermoelectric figure of merit in the same order, and could be important for piezoresistive applications. © *2011 American Institute of Physics*. [doi:10.1063/1.3669446]

I. INTRODUCTION

The performance of CMOS devices is inextricably linked to the mobility of their active regions. Higher mobility results in faster switching times and lower power consumption. There are several ways in which these two desirable properties have been achieved in the past. To mention a few, the reduction in device size, the incorporation of higher mobility materials, and strain engineering have all successfully been applied to CMOS technology. However, having reached the size limits possible in this technology and with the scarcity of new materials compatible with the CMOS fabrication process, the further increase in performance has largely relied on strained architectures.

The carrier mobility is also important in thermoelectric applications. Increasing the mobility by strain in these alloys results in an increase of the thermoelectric figure of merit,[1] $Z = S^2\sigma/\kappa$, where S is the Seebeck coefficient, σ the electrical conductivity, and κ the thermal conductivity. The change in the thermal conductivity and the Seebeck coefficient are expected to be small compared to the change produced in the electrical conductivity by strain. Since $\sigma = ne\mu$, with μ the mobility and n the carrier occupation, an increase in mobility is accompanied by the same increase in the thermoelectric figure of merit.

Furthermore, the rate of change in the mobility is related to the performance of piezoresistive applications. The piezoresistance gauge factor gives a measure of the sensitivity of a piezoresistive device. The gauge factor G is proportional to the rate of change of the conductivity with strain, $G = -\Delta\sigma/(\sigma\varepsilon)$, where ε is the strain.[2] Thus, the larger the change in conductivity with strain the more sensitive a piezoresistive sensor is.

In Si, Ge, and their alloy, the mobility can be substantially enhanced by the application of small amounts of strain, resulting in the lowering (raising) of a conduction (valence) band valley with a lower effective mass in the direction of transport and a reduction in inter-valley scattering. The increase in mobility will thus depend on the symmetry of the band and that of the strain applied, the amount of strain and the direction of transport.[3]

To predict the effects of strain on the material properties, a thorough understanding is needed of the relative importance of various scattering mechanisms and how they are affected by strain. While carrier mobility measurements in bulk systems provide much information, they do not always uniquely determine the separate contributions.[3,4] Therefore, a method to theoretically predict the charge transport properties from only a knowledge of the atomic positions is of practical and physical importance. Many works[3,5–11] have explored the effects of strain on these alloys using empirical or phenomenological models. However, it has been shown[4] that phenomenological models of the scattering parameters do not give the correct ratio of intra- to inter-valley scattering. Getting this ratio right is important when one of these scattering mechanisms is suppressed by strain.

Our aim in this paper is to include the effects of strain in our recently developed first principles methods[4,12,13] to calculate the alloy and electron-phonon scattering parameters in SiGe and apply them to map the *n*-type carrier mobility enhancement as a function of strain configuration and SiGe alloy composition. A further contribution of this work is the validation of the deformation potential approach in strained systems against the full electron-phonon scattering matrix treatment. We find that strain can enhance the mobility from two to eleven times that of the unstrained alloy, at a desired composition. In absolute terms, however, the mobility is still largely hampered by alloy scattering, so the largest values of the mobility are obtained for strained Ge.

II. BANDS AND STRAIN

The conduction band minimum of Si is located along the Δ crystallographic line and is composed of six degenerate

a)Author to whom correspondence should be addressed. Electronic mail: philip.murphy@tyndall.ie.

equivalent valleys in the $[00\xi]$, $[00\bar{\xi}]$, $[0\xi0]$, $[0\bar{\xi}0]$, $[\xi00]$, $[\bar{\xi}00]$ crystallographic directions, where $\xi = 0.83\frac{2\pi}{a_0}$ and a_0 is the cubic lattice constant. The conduction band minimum of Ge is located at the L point in the Brillouin zone, with four equivalent valleys at $\frac{\pi}{a_0}[111]$, $\frac{\pi}{a_0}[\bar{1}11]$, $\frac{\pi}{a_0}[1\bar{1}1]$, and $\frac{\pi}{a_0}[11\bar{1}]$ (see Figure 1). For $Si_{1-x}Ge_x$ with $x < 0.85$, the conduction band valleys are Si-like, otherwise they are Ge-like. All the conduction band valleys have parabolic energy dispersions, with two effective masses: m_l along the crystallographic direction of the valley and $m_t << m_l$ perpendicular to it.

The effects of strain on the electronic structure of an fcc lattice such as SiGe can be understood from the deformation potential theory developed by Herring and Vogt.[14] The shifts in the Δ valley at $[\xi00]$ and the L valley at $\frac{\pi}{a_0}[111]$ due to strain are given by

$$\Delta E_c^{\Delta} = \left(\Xi_d^{\Delta} + \frac{1}{3}\Xi_u^{\Delta}\right)(e_1 + e_2 + e_3) + \frac{1}{3}\Xi_u^{\Delta}[(e_1 - e_2) + (e_1 - e_3)], \quad (1)$$

$$\Delta E_c^{L} = \left(\Xi_d^{L} + \frac{1}{3}\Xi_u^{L}\right)(e_1 + e_2 + e_3) + \frac{1}{3}\Xi_u^{L}(e_4 + e_5 + e_6), \quad (2)$$

respectively, where Ξ_d and Ξ_u are the dilatational and uniaxial deformation potentials, and e_i are the Cartesian strain tensor components defined as

$$\begin{aligned} e_1 &= \varepsilon_{xx}; & e_2 &= \varepsilon_{yy}; \\ e_3 &= \varepsilon_{zz}; & e_4 &= \varepsilon_{xy} + \varepsilon_{yx}; \\ e_5 &= \varepsilon_{zy} + \varepsilon_{yz}; \\ e_6 &= \varepsilon_{zx} + \varepsilon_{xz}. \end{aligned} \quad (3)$$

Therefore, strain in the [100] direction of magnitude ε results in $e_1 = \varepsilon$ and $e_2 = e_3 = e_4 = e_5 = e_6 = 0$. Likewise, strain in the [111] direction yields $e_1 = e_2 = e_3 = e_4/2 = e_5/2 = e_6/2 = \varepsilon$. Strain in the $[\bar{1}11]$ direction yields $e_1 = e_2 = e_3 = -e_4/2 = e_5/2 = -e_6/2 = \varepsilon$, and so on.

It is easily seen that strain in the [100] axis will lift the degeneracy of the $[\xi00]$ and $[\bar{\xi}00]$ valleys from the $[0\xi0]$, $[0\bar{\xi}0]$, $[00\xi]$, and $[00\bar{\xi}]$ Δ valleys, while the four L valleys remain degenerate. Correspondingly, [111] strain removes the $\frac{\pi}{a_0}[111]$ L valley from the quadruplet, and the Δ valleys remain degenerate. The lifting of the degeneracy of the various valleys is the most important effect increasing the mobility in SiGe.

We have also included in our analysis the effects of strains on the Γ band, which have been treated elswhere.[15]

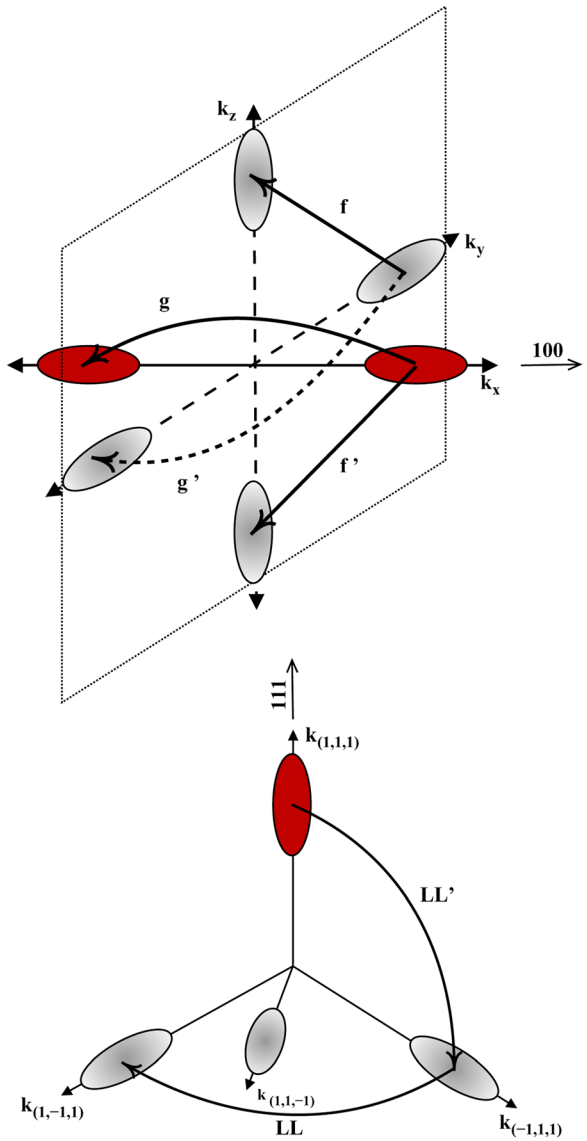

FIG. 1. (Color online) The surfaces of constant energy in the Δ valleys (upper panel) and L valleys (lower panel) for SiGe alloys. The inter-valley f-type and inter-valley g-type scattering matrix elements are indicated by lines between the Δ valleys, and the inter-valley LL scattering matrix elements by a line between two of the L valleys. The primed labels indicate a matrix element between valleys that are degenerate in the unstrained case, but are no longer equivalent when the crystal is strained in the $\langle 100\rangle$ or $\langle 111\rangle$ direction for the Δ and L valleys, respectively.

III. PHONON SCATTERING

A. Intra-valley scattering

We calculate the full electron-phonon (el-ph) matrix element using the frozen phonon approach, as discussed in Ref. 13. For the unstrained system, we find that the deformation potential approach gives an excellent fit to the full el-ph matrix for long wavelength phonons. In Deformation Potential Theory, the dependence of the el-ph matrix on phonon momentum q is assumed to be linear, and in Fig. 1 we observe that this holds true for the el-ph matrix elements due to long-wavelength phonons (wavelength $> 10a_0$). This approach continues to be good for the strained system, with the inclusion of corrections up to second order in strain. These corrections may be calculated by perturbation theory from the second term in the following expansion of the energy shift in terms of the strain:[16]

$$\delta E = \sum_{i=1}^{6}\left(\frac{\partial E}{\partial e_i}e_i + \sum_{j=1}^{6}\frac{\partial^2 E}{\partial e_i \partial e_j}e_i e_j\right). \quad (4)$$

From group theory, we can work out that six additional terms to Eq. (1) are needed to account for the second order energy shifts in the Δ and L valleys, so that the total shifts are given by

$$\begin{aligned}\delta E_{100} = &\left(\Xi_d^{\Delta} + \frac{1}{3}\Xi_u^{\Delta}\right)(e_1 + e_2 + e_3) \\ &+ \frac{1}{3}\Xi_u^{\Delta}[(e_1 - e_2) + (e_1 - e_3)] + A^{\Delta}\left(e_2^2 + e_3^2\right) \\ &+ B^{\Delta}e_1^2 + C^{\Delta}e_2e_3 + D^{\Delta}(e_1e_3 + e_1e_2) \\ &+ E^{\Delta}e_5^2 + F^{\Delta}\left(e_4^2 + e_6^2\right),\end{aligned} \tag{5}$$

for the [100] Δ valley and

$$\begin{aligned}\delta E_c^L = &\left(\Xi_d^L + \frac{1}{3}\Xi_u^L\right)(e_1 + e_2 + e_3) + \frac{1}{3}\Xi_u^L(e_4 + e_5 + e_6) \\ &+ A^L\left(e_1^2 + e_2^2 + e_3^2\right) + B^L(e_1e_2 + e_1e_3 + e_2e_3) \\ &+ C^L(e_1e_4 + e_2e_5 + e_3e_6 + e_1e_6 + e_2e_1 + e_3e_5) \\ &+ D^L(e_1e_5 + e_2e_6 + e_3e_4) + E^L\left(e_4^2 + e_5^2 + e_6^2\right) \\ &+ F^L(e_4e_6 + e_4e_5 + e_5e_6),\end{aligned} \tag{6}$$

for the [111] L valley, where A^i, B^i, C^i, D^i, E^i, and F^i are the second order deformation potentials of valley i. The shifts for the other equivalent valleys can be easily obtained by permuting the e_i.

1. Frozen phonon calculations

In the deformation potential approach, the effect of a long-wavelength phonon on the electronic bands is assumed to be equivalent to a slowly varying potential, arising from the displacements $\delta\mathbf{R}$ of the atoms from their equilibrium positions due to the presence of a phonon of momentum $\mathbf{q}$,

$$\delta\mathbf{R}(\mathbf{r}) = \delta\mathbf{R}_0 \sin(\mathbf{q}\cdot\mathbf{r} - \omega t). \tag{7}$$

The strain produced by this displacement is given by[17]

$$\varepsilon_{ij}(\mathbf{r}) = \frac{1}{2}\left(\frac{\partial\delta R_i}{\partial r_j} + \frac{\partial\delta R_j}{\partial r_i}\right), \tag{8}$$

where δR_i is the ith Cartesian component of the atomic displacement vector at $\mathbf{r}$. More explicitly, Eq. (8) becomes

$$\varepsilon_{ij}(\mathbf{r}) = \frac{1}{2}(q_i\delta R_{0j} + q_i\delta R_{0j})\cos(\mathbf{q}\cdot\mathbf{r} - \omega t). \tag{9}$$

Inserting Eq. (9) into Eq. (6), the matrix element of $\langle\mathbf{k}|\delta E_L|\mathbf{k}'\rangle$ with electron states $|\mathbf{k}\rangle$ and $|\mathbf{k}'\rangle$ at $t=0$ will contain terms with

$$\langle\mathbf{k}|\cos(\mathbf{q}\cdot\mathbf{r})|\mathbf{k}'\rangle = \frac{\delta_{\mathbf{k}-\mathbf{k}',\mathbf{q}} + \delta_{\mathbf{k}'-\mathbf{k},\mathbf{q}}}{2} \tag{10}$$

and

$$\langle\mathbf{k}|\cos^2(\mathbf{q}\cdot\mathbf{r})|\mathbf{k}'\rangle = \frac{\delta_{\mathbf{k}-\mathbf{k}',2\mathbf{q}} + \delta_{\mathbf{k}'-\mathbf{k},2\mathbf{q}}}{4} + \frac{\delta_{\mathbf{k}',\mathbf{k}}}{2}. \tag{11}$$

We can obtain the deformation potentials by calculating the electron-phonon matrix element from first principles. For example, a longitudinal phonon in the $\hat{x}$ direction, which introduces a strain $e_1 = \delta R_0 q\cos(qx)$, will produce the electron-phonon matrix element between states $|\mathbf{k}\rangle$ and $|\mathbf{k}+\boldsymbol{q}\rangle$ of band E_L,

$$\langle\mathbf{k}|\delta E_L|\mathbf{k}+\mathbf{q}\rangle = \frac{1}{2}\Xi_1\delta R_0 q, \tag{12}$$

yielding as a result the deformation potential Ξ_1 for the L valley. In like manner, introducing a uniform strain e_1' in the x direction, the total strain becomes

$$e_1 = \delta R_0 q\cos(qx) + e_1', \tag{13}$$

and hence the matrix element,

$$\langle\mathbf{k}|\delta E_L|\mathbf{k}+\mathbf{q}\rangle = \left(\frac{1}{2}\Xi_1 + Ae_1'\right)\delta R_0 q. \tag{14}$$

We notice in Eq. (14) that the effect of a uniform strain on the crystal is to introduce a change in the deformation potential proportional to that strain. These quantities can be readily extracted from supercell frozen phonon calculations at different values of $\mathbf{q}$ and $\mathbf{e}'$, as in Ref. 13, Section C. As seen in Fig. 2, the el-ph matrix elements are linear in q for long-wavelength phonons, and higher order terms in q can be neglected with little effect on the overall scattering. As we shall see later, the quadratic dependence on strain is in some cases comparable to the linear part and has to be included in the calculation of the mobility.

B. Inter-valley scattering

The effect of strain on inter-valley scattering transitions depends on their symmetry. In the unstrained case, there are two types of inter-valley scattering at the Δ valley, namely g- and f-type for transitions along and perpendicular to the valley axis, respectively, and one for L valley scattering. Strain along the [100] direction affects the scattering parameters in the following way (see Fig. 1):

(i) There is an additional type of g-type scattering, depending on whether the transition is parallel or perpendicular to the strain direction.

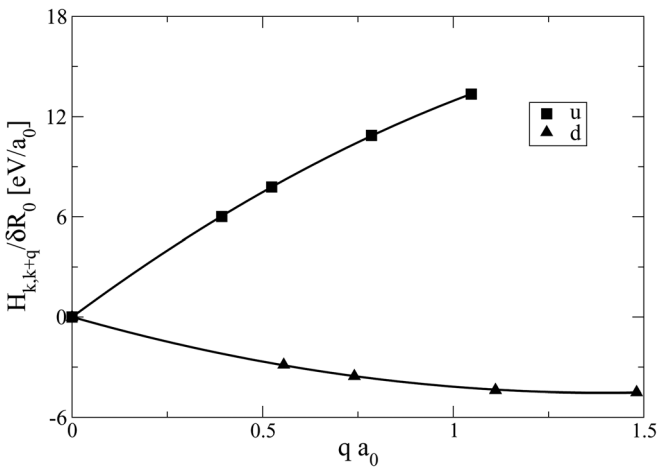

FIG. 2. First principles electron-phonon matrix element vs $\mathbf{q}$ for unstrained Ge, calculated using the frozen phonon approach. The slopes, as $\mathbf{q}\to 0$, yield the deformation potentials, Ξ_d and Ξ_u, for the L valley.

(ii) There is an additional type of *f*-type scattering, between the now inequivalent valleys.
(iii) There is an additional type of *L*-type scattering, depending on whether the momentum change is parallel or perpendicular to the strain direction.

Likewise, strain in the [111] direction introduces:

(iv) An additional type of *L*-type scattering, between the now inequivalent valleys.
(v) An additional type of *f*-type scattering, depending on whether the momentum change is parallel or perpendicular to the strain direction.

Under tensile strain, the Γ valley lowers in energy faster than the *L* valley. The strains considered here are not enough for the Γ valley to become the lowest conduction band valley. However, due to their proximity, we have considered the scattering between the *L*, Δ, and Γ valleys.

IV. ALLOY SCATTERING

As in the case for electron-phonon scattering, the effect of strain can be separated into intra- and inter-valley contributions. The same symmetry treatment applies for inter-valley alloy scattering as for inter-valley scattering by phonons. As strain breaks the degeneracy of the original valleys, so it changes the value of the intra-valley scattering parameters belonging to these valleys. We shall calculate these values directly, following the methods used in Refs. 4 and 13.

V. METHOD

To calculate the alloy and el-ph scattering parameters, we employ the methods of Refs. 4 and 13. The calculation of the effects of strain on the el-ph matrix elements requires performing the frozen phonon calculation under strain in the [100], [110], and [111] directions. The different second order deformation potentials are obtained by applying these strains to phonons in particular directions and branches. Table I shows the required combinations of strain and phonon wavevector, which yield the deformation potentials for the Δ and *L* valleys.

TABLE I. Combination of phonon momentum, polarization, and strain tensor to obtain the different second order deformation potentials for the Δ and *L* valleys.

Def. Pot.	Valley	$\hat{q}$	$\delta\hat{R}_0$	e
A	Δ	010	010	e_2
	L	100	100	e_1
B	Δ	100	100	e_1
	L	010	010	e_1
C	Δ	010	010	e_3
	L	010	100	e_1
D	Δ	100	100	e_3
	L	010	100	e_3
E	Δ	010	001	e_5
	L	010	100	e_4
F	Δ	100	010	e_4
	L	010	100	e_5

All the calculations of the band structure have been performed with the Abinit code.[18–20] We use the local density approximation (LDA) for exchange and correlation. FHI pseudopotentials of the Trouiller-Martins type (available in the Abinit website[19]) are used for all calculations in this paper. We use an energy cut-off of 18 Hartree for the expansion of wavefunctions in all our calculations, except for those of the second order deformation potentials, which require a cut-off of 43 Hartree. The supercell sizes are the same as described in Ref. 13. The required number of Monkhorst-Pack irreducible k-points for the first and second order deformation potentials is 134 and 198, respectively. The convergence criteria for the calculation of second order deformation potentials are more stringent than in the case of Ref. 13, since the parameters are obtained from the difference with the unstrained deformation potentials. The GW approximation[21] is used to obtain the band energy differences between the Δ, *L*, and Γ valleys.

VI. RESULTS

A. Scattering parameters

The electron-phonon and alloy scattering parameters have been calculated from first principles including the effects of strain. The intra-valley el-ph matrix elements are found to depend up to second order in strain, therefore the deformation potential approach requires no further corrections. Table II shows the second order deformation potentials for the Δ and *L* valleys in SiGe. Except for the *E* deformation potential for the Δ valley, all other values will have little influence on the overall scattering. As implied by Eq. (5), scattering of type *E* will increase electron phonon scattering drastically only when strain components e_{ij}, with $i \neq j$ are present, as is the case for [111] and [110] strains.

The fractional variation of the alloy scattering parameters with strain is on the same order as the strain, and has little influence on the overall mobility. The same is true for the inter-valley electron-phonon scattering parameters, except the *L* to *L* scattering, which changes by 25% for 1% strain. However, this type of scattering is very small in comparison to acoustic phonon and alloy scattering, resulting in no perceptible change in the mobility.

We have considered the inter-valley electron-phonon scattering of the *L* and Δ valleys with the Γ valley. The calculated Γ intra-valley and $\Gamma - L$ and $\Gamma - \Delta$ inter-valley alloy scattering parameters labelled V_Γ, $V_{\Gamma L}$, and $V_{\Gamma\Delta}$, respectively, are shown in Table III. The calculated inter-valley

TABLE II. Calculated second order deformation potentials for the calculation of the electron-phonon scattering.

	Δ(eV)	*L*(eV)
A	−5	17
B	3	−23
C	−4	6
D	5	−27
E	197	−4
F	0	−14

TABLE III. Calculated Γ intra-valley and $\Gamma - L$ and $\Gamma - \Delta$ inter-valley alloy scattering parameters, denoted by V_i, and $\Gamma - L$ and $\Gamma - \Delta$ inter-valley deformation potentials, denoted by D_i.

	Value
V_Γ (eV)	1.28
$V_{\Gamma L}$ (eV)	0.82
$V_{\Gamma\Delta}$ (eV)	0.38
$D_{\Gamma L}$ (eV/Å)	4.1
$D_{\Gamma\Delta}$ (eV/Å)	2.5

electron-phonon scattering parameters are $D_{\Gamma L} = 4.1$ eV/Å and $D_{\Gamma\Delta} = 2.5$ eV/Å, also shown in Table III, which are in excellent agreement with previous calculated[22] and experimental[23,24] values.

B. *n*-type carrier mobility

We have computed the *n*-type carrier mobility in a bulk strained SiGe alloy using the calculated scattering parameters in the Boltzmann Transport Equation within the relaxation time approximation.[13] We have considered the mobility enhancement produced by two types of uniaxial strain, namely, in the [100] and [111] directions up to ±1% strain. The transport directions were chosen to highlight the highest mobility enhancement possible when transport occurs along the direction with the lowest effective mass. For the [100] strain, we have calculated the mobility enhancement for transport in the [100] and [010] directions. For strain in the [111] direction, the chosen transport directions were [110] and $[1\bar{1}0]$.

The results are shown in Figs. 3–6. From the figures it is clear that strain can do little to suppress the very strong alloy scattering. The expected effect of mobility increase in Si-like SiGe with [100] strain can be observed in Fig. 3. Compressive strain in the [100] direction lifts four of the six Δ valleys in energy. If current is allowed to flow in the direction of the lightest effective mass, i.e., perpendicular to the strain direction, the mobility increases two- to fourfold (see Fig. 7). For an illustration of how *f*-type phonon and alloy scattering affect the mobility for Si-like alloy compositions, compare Figs. 7 and 8, which represent the mobility enhancements for the cases in Figs. 3 and 4, respectively. In the first case, compressive strain lowers two of the six valleys in energy, removing all sources of *f*-type scattering. In the second case,

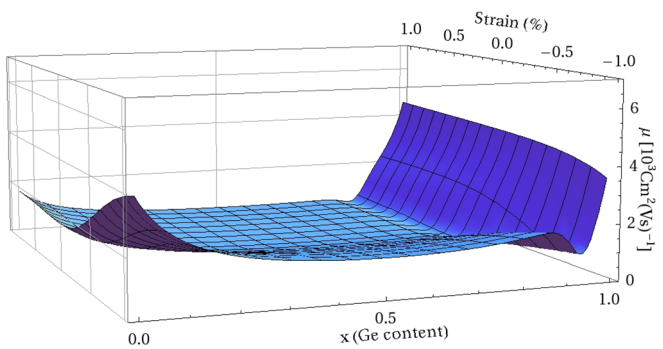

FIG. 3. (Color online) Mobility of $Si_{1-x}Ge_x$ strained uniaxially in the [100] direction, with transport along the [010] direction.

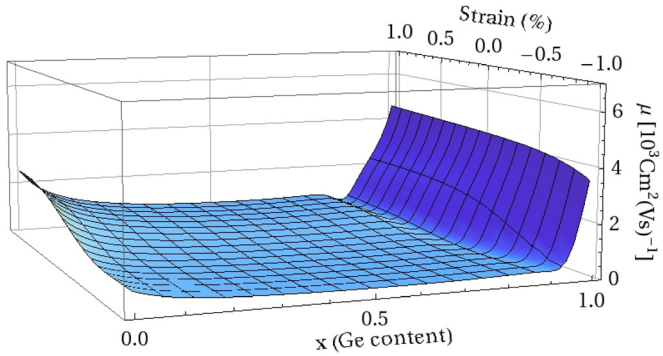

FIG. 4. (Color online) Mobility of $Si_{1-x}Ge_x$ strained uniaxially in the [100] direction, with transport along the [100] direction.

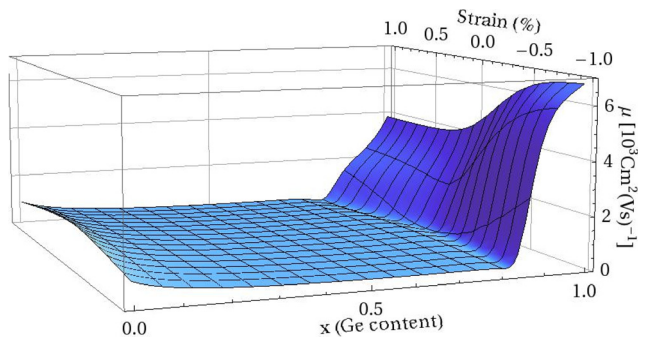

FIG. 5. (Color online) Mobility of $Si_{1-x}Ge_x$ strained uniaxially in the [111] direction, with transport along the $[1\bar{1}0]$ direction.

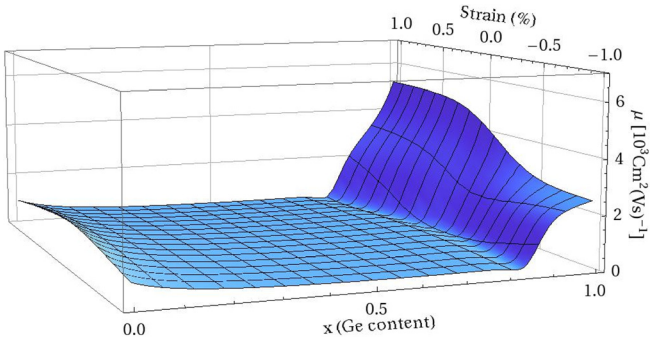

FIG. 6. (Color online) Mobility of $Si_{1-x}Ge_x$ strained uniaxially in the [111] direction, with transport along the [110] direction.

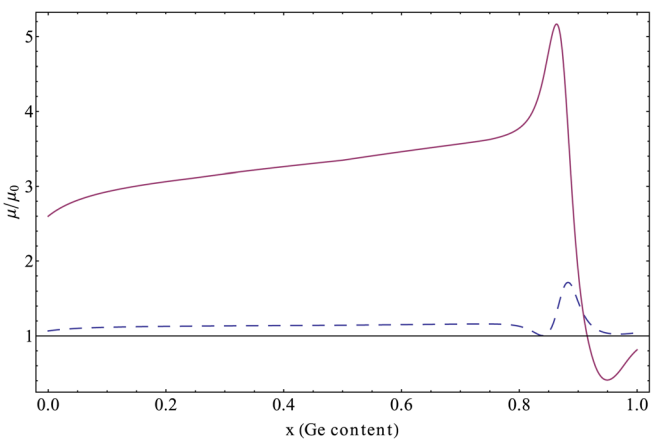

FIG. 7. (Color online) Mobility enhancement of strained SiGe over unstrained SiGe as a function of Ge content, for $\varepsilon_{xx} = -0.01$ (solid line) and $\varepsilon_{xx} = 0.01$ (dashed line), with transport in the [010] direction.

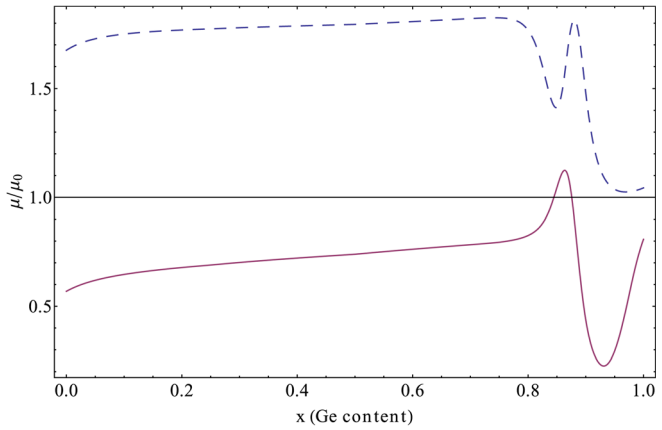

FIG. 8. (Color online) Mobility enhancement of strained SiGe over unstrained SiGe as a function of Ge content, for $\varepsilon_{xx} = -0.01$ (solid line) and $\varepsilon_{xx} = 0.01$ (dashed line), with transport in the [100] direction.

tensile strain lowers four of the six valleys, and *f*-type scattering remains present. In both cases, transport is through the lower effective mass direction. The mobility enhancement in the first case is 50% larger than the second case for pure Si, and nearly twice as much for alloy compositions of $x \sim 0.5$, due to the increased alloy *f*-type scattering in the latter case. This type of strain does not affect the degeneracy of the *L* Ge-like valleys.

The *L* valleys are split in energy by [111] strain. Compressive strain in this direction lifts three of the four *L* valleys in energy. The conduction band minimum in Ge-like SiGe is therefore located at the $\frac{\pi}{a_0}(1,1,1)$ valley, with the lightest effective mass transverse to this direction. If, for example, transport is confined to the $[1\bar{1}0]$ direction, the mobility at -1% strain will be 40% larger than in the unstrained case, and 4 times larger than that of unstrained Si, as seen in Figs. 5 and 9. Tensile strain in the [111] direction, with transport along the [110] direction can only achieve an increase in the mobility of 10% for pure Ge, as it is not possible to effect transport along the lowest effective mass direction (see Fig. 10). While the degeneracy of the Δ valleys is not affected by this type of strain, the non-linearities in the elph coupling with strain (second order deformation potentials)

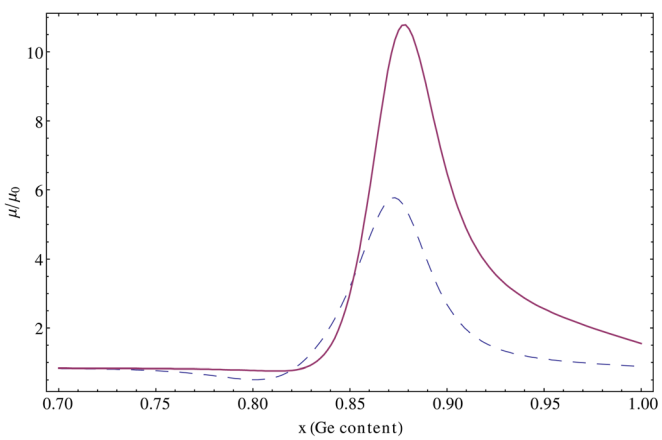

FIG. 9. (Color online) Mobility enhancement of strained SiGe over unstrained SiGe as a function of Ge content, for $\varepsilon_{111} = -0.01$ (solid line) and $\varepsilon_{111} = 0.01$ (dashed line), with transport in the $[1\bar{1}0]$ direction.

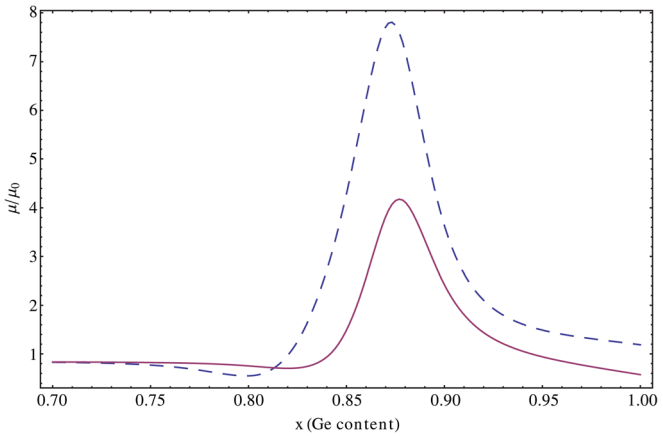

FIG. 10. (Color online) Mobility enhancement of strained SiGe over unstrained SiGe as a function of Ge content, for $\varepsilon_{111} = -0.01$ (solid line) and $\varepsilon_{111} = 0.01$ (dashed line), with transport in the [110] direction.

increase the electron-acoustic phonon scattering, reducing the Si-like mobility by almost half.

It is interesting to see what happens to the mobility of Ge-like SiGe under tensile [111] strain. Irrespective of the transport direction, tensile (compressive) strain lowers three (one) of the four *L* valleys with respect to the Δ valley, resulting in the Si- to Ge-type alloy crossing over lower than $x = 0.85$. This increases the mobility of SiGe from four to eleven times the unstrained case for compositions between $0.80 \leq x \leq 0.90$, as seen in Figs. 9 and 10.

The effect on the mobility of applying higher compressive strains would in general continue the same trends observed for up to -1%. Large tensile strains, however, cause the Γ valley to cross below the *L* valley in pure Ge, potentially increasing the mobility enormously, due to the much smaller effective mass and scattering rates of the Γ valley. The effects of this type of strain on Ge have been treated elsewhere.[15]

VII. CONCLUSIONS

We have calculated the mobility of strained SiGe alloys from first principles. The earlier method[13] for calculating scattering in semiconductor alloys has been expanded to include the effects of strain on the phonon and alloy scattering parameters. We find increases in mobility of up to 11 times at 1% strain, at fixed alloy compositions, for both tensile and compressive strain. These enhancements in mobility could prove important in defining the best strain configuration to use SiGe for piezoresistive and thermoelectric applications.

We find that the deformation potential approach is an excellent approximation, even for strained systems, compared to using the full electron-phonon matrix. Non-linear terms in the deformation potentials are found in general not to be important, except for the Δ valley in SiGe under shear strain, which results in a drastic decrease in mobility. The influence of strain on the alloy scattering parameters is found to be small (within 1%) for the strains considered here.

ACKNOWLEDGMENTS

This work has been supported by Science Foundation Ireland.

[1]M. S. Dresselhaus, G. Chen, M. Y. Tang, R. Yang, H. Lee, D. Wang, Z. Ren, J. P. Fleurial, and P. Gogna, Adv. Mater. **19**, 1 (2007).
[2]Y. Kanda, IEEE Trans. Electron Devices **29**, 64 (1982).
[3]M. Fischetti and S. Laux, J. Appl. Phys. **80**, 2234 (1996).
[4]F. Murphy-Armando and S. Fahy, Phys. Rev. Lett. **97**, 096606 (2006).
[5]F. M. Bufler, P. Graf, B. Meinerzhagen, B. Adeline, M. M. Rieger, H. Kibbel, and G. Fischer, IEEE Electron Device Lett. **18**, 264 (1997).
[6]T. Manku and A. Nathan, IEEE Trans. Electron Devices **39**, 2082 (1992).
[7]M. M. Rieger and P. Vogl, Phys. Rev. B **48**, 14276 (1993).
[8]M. Michaillat, D. Rideau, F. Aniel, C. Tavernier, and H. Jaouen, Thin Solid Films **518**, 2437 (2010).
[9]A. T. Pham, C. Jungemann, and B. Meinerzhagen, IEEE Trans. Electron Devices **54**, 2174 (2007).
[10]B. Senapati, IETE J. Res. **53**, 215 (2007).
[11]S. Smirnov and H. Kosina, Solid-State Electron. **48**, 1325 (2004).
[12]S. Joyce, F. Murphy-Armando, and S. Fahy, Phys. Rev. B **75**, 155201 (2007).
[13]F. Murphy-Armando and S. Fahy, Phys. Rev. B **78**, 035202 (2008).
[14]C. Herring and E. Vogt, Phys. Rev. **101**, 944 (1956).
[15]F. Murphy-Armando and S. Fahy, J. Appl. Phys. **109**, 113703 (2011).
[16]F. Murphy-Armando and S. Fahy, Chin. J. Phys. **49**, 209 (2011).
[17]P. Yu and M. Cardona, *Fundamentals of Semiconductors* (Springer, Berlin, 2001), pp. 121–136.
[18]X. Gonze, B. Amadon, P.-M. Anglade, J.-M. Beuken, F. Bottin, P. Boulanger, F. Bruneval, D. Caliste, R. Caracas, M. Cote, T. Deutsch, L. Genovese, P. Ghosez, M. Giantomassi, S. Goedecker, D. Hamann, P. Hermet, F. Jollet, G. Jomard, S. Leroux, M. Mancini, S. Mazevet, M. Oliveira, G. Onida, Y. Pouillon, T. Rangel, G.-M. Rignanese, D. Sangalli, R. Shaltaf, M. Torrent, M. Verstraete, G. Zerah, and J. Zwanziger, Comput. Phys. Commun. **180**, 2582 (2009).
[19]X. Gonze, G.-M. Rignanese, M. Verstraete, J.-M. Beuken, Y. Pouillon, R. Caracas, F. Jollet, M. Torrent, G. Zerah, M. Mikami, P. Ghosez, M. Veithen, J.-Y. Raty, V. Olevano, F. Bruneval, L. Reining, R. Godby, G. Onida, D. Hamann, and D. Allan, Z. Kristallogr. **220**, 558 (2005).
[20]The ABINIT code is a common project of the Université Catholique de Louvain, Corning Incorporated, and other contributors (http://www.abinit.org).
[21]M. S. Hybertsen and S. G. Louie, Phys. Rev. B **34**, 5390 (1986).
[22]V. Tyuterev, S. Obukhov, N. Vast, and J. Sjakste, Phys. Rev. B **84**, 035201 (2011).
[23]G. Li, A. Goñi, K. Syassen, and M. Cardona, Phys. Rev. B **49**, 8017 (1994).
[24]X. Zhou, H. van Driel, and G. Mak, Phys. Rev. B **50**, 5226 (1994).